Particle Deposition Study During Sessile Drop Evaporation

Ervina Widjaja and Michael T. Harris
School of Chemical Engineering, Purdue University, West Lafayette, IN 47907

DOI 10.1002/aic.11558
Published online July 10, 2008 in Wiley InterScience (www.interscience.wiley.com).

The focus of this article is the numerical study of particle deposition profiles on a solid substrate during the evaporation of a sessile drop of a colloidal particle suspension. The evaporation flux along the drop interface, the induced fluid dynamics inside the drop, and the particle deposition profile on the solid substrate are solved simultaneously. The governing equations are solved numerically using the Galerkin/finite element method (G/FEM) for discretization of the spatial domain and an adaptive finite difference method for discretization in the time domain. Several particle deposition profiles, such as a ring-shaped deposit and uniform particle distribution, are obtained from the numerical simulations. The particle deposition profile is found to be influenced by the mass transfer (both convective and diffusive mass transfer) of the particles in the bulk liquid and by the deposition rate along the substrate. © 2008 American Institute of Chemical Engineers *AIChE J,* 54: 2250–2260, 2008
Keywords: sessile drop evaporation, particle deposition profile, evaporation flux calculation, fluid dynamics, finite element analysis

Introduction

There has been considerable interest in utilizing the sessile drop evaporation method to deposit particles on a solid substrate. This method has been applied to create an ordered array of semiconductor nanoparticles for electronic application[1] and of DNA molecules for gene expression analysis.[2] Different deposition profiles are desired based on the functionalities of the deposits. For ink deposition, a uniform particle distribution is desired, for DNA deposition, a stretched individual particle is desired,[3] and for other applications, ordered arrays of ring-shaped deposits are desired.[1] We would like to understand which parameters control the particle deposition profile on the substrate.

This deposition method is simple, when a drop containing particles is placed on a solid substrate, the solvent will evaporate and the particles will be deposited on the substrate. Another advantage of using this method is the possibility of creating an array of sessile droplets by using the inkjet printing method. Recognizing the importance of sessile drop evaporation for particle deposition applications, people have been interested in the theoretical understanding of this process.

Sessile drop evaporation is a complex problem which includes three different phases; the vapor around the drop, the liquid drop, and the particles which are suspended in the liquid. The investigation of the evaporation dynamics, which focused only on the vapor area outside the drop, have been done analytically by Picknett and Bexon[4] and numerically by Hu and Larson[5] These methods can be applied to predict the evaporation rate of different liquids.

The influence of the evaporation dynamics on the fluid dynamics inside the drop has been studied numerically by Hu and Larson[6] and Widjaja and Harris[7] In these studies, the system includes the liquid drop and the area outside the drop, the evaporation flux, the drop shape, and the fluid flow profiles.

The theoretical study of the particle deposition during sessile drop evaporation has been done by Deegan et al.,[8] Fischer,[9] Chopra et al.,[2] and Popov.[10] Deegan et al.[8] and Popov[10] considered a very thin drop. They derived a height-averaged radial velocity and neglected the vertical flow that

Correspondence concerning this article should be addressed to M. T. Harris at mtharris@ecn.purdue.edu.

is present in the drop; the particles were swept radially to the contact line of the drop. Fischer[9] also considered very thin droplets. He used the lubrication approximation to simplify the governing equations. The particle concentration distribution is also driven solely by convective mass transfer, the particle diffusion is neglected. In those studies mentioned, the particle distribution is calculated in the liquid bulk, they did not calculate the amount of particle deposited or transferred from the liquid bulk to the substrate during evaporation. Chopra et al.[2] used Brownian dynamics simulation to predict the stretching and the deposition on DNA onto a substrate. For deposition, Chopra considered irreversible DNA adsorption by freezing the location of any bead that comes into contact with the substrate surface.

In this study, we would like to calculate the particle deposition distribution on the substrate. Several ways of describing the boundary conditions which describe the deposition of particles on the substrate have been mentioned in the previous works. Spielman and Friedlander,[11] Ruckenstein and Prieve,[12] and Bowen et al.[13] used the perfect sink boundary condition. The particle concentration on the substrate is set to be zero, so all particles reaching the surface are removed from the dispersed phase. In this article, the deposition boundary condition takes the form of an irreversible first-order chemical reaction on the surface as described by Spielman et al.,[11] and Ruckenstein and Prieve.[12,14] The particles are removed as they touch the solid substrate at a defined deposition rate. The deposition rate defines how fast the particles are transferred from the bulk fluid to the solid surface. The simplistic model that is used for the particle deposition rate on the substrate allows best qualitative results for the particle deposition profile. A thorough study of the particle substrate interactions needs to be done and a particle deposition model that captures more of the physics and chemistry is required to yield more quantitative results. Furthermore, the deposited particles will alter the topology of the substrate surface which will influence the flow profile of the fluid. These effects were not captured in the research that is presented in this manuscript.

In this study the evaporation flux along the drop interface, the induced fluid dynamics inside the drop, and the particle deposition profile on the solid substrate are solved simultaneously. The governing equations are solved numerically using the Galerkin/finite element method (G/FEM) for discretization of the spatial domain and an adaptive finite difference method for discretization in the time domain. Convective and diffusive mass transfer in the bulk liquid are considered. We would also like to understand which parameters control the particle deposition profile on the substrate.

Formulation of the Problem

System description

The schematic of the system is shown on Figure 1. The system is an axisymmetric sessile droplet of an incompressible, Newtonian liquid of spatially uniform and constant viscosity (μ) and density (ρ) and the dynamically inactive vapor above the drop with spatially uniform and constant vapor diffusivity (D_v). The ambient fluid exerts a uniform pressure and negligible viscous drag on the droplet. The surface tension (σ) of the liquid–gas interface is spatially uniform and constant. No temperature gradient is assumed here. The aspect ratio of the droplet is obtained by dividing the height of the drop (h) by the fixed radius at the contact line (R).

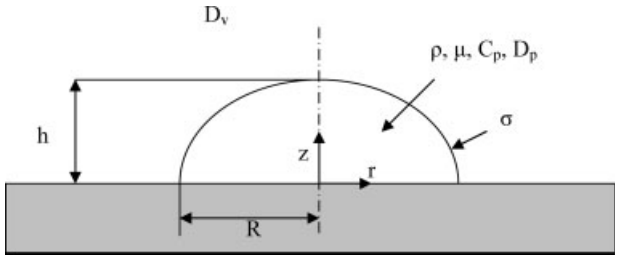

Figure 1. Schematic of a sessile drop of particle suspension sitting on a solid substrate surrounded by dynamically inactive vapor.

On the interface of the drop, the vapor concentration ($\tilde{c}$) is set to be the saturated vapor concentration (c_v) and far away from the interface the vapor concentration will be defined later. Initially, the sessile droplet is sitting on a solid substrate at its equilibrium configuration and is determined from solution of the Young-Laplace equation. The drop is a very dilute suspension of small particles, with initial particle concentration ($\tilde{C}_p$) of C_o to be set everywhere in the liquid. Particle diffusivity is D_p. The particles deposit rate is modeled as a first-order rate expression with deposition rate constant k_d, k_d is influenced by particle-substrate interaction.[11,12,14] In this study, the calculation is done until drop contact angle decreases to 5°. Hu and Larson[5] observed experimentally that the water drop contact line is fixed during evaporation process until the contact angle reaches 2°–4°, then the contact line starts to recede. It is acceptable in this study to assume that the contact line is fixed throughout the evaporation process.

Reference scales

The flow of the liquid is governed by the Stokes system. The characteristic length is the droplet radius at the pinned contact line, $l_c = R$, the characteristic vapor concentration is the saturated vapor concentration, $c_c = c_v$, the characteristic particle concentration is the initial particle concentration, $C_c = C_o$. From the kinematic boundary condition, the characteristic velocity is obtained to be $v_c \equiv J_o/\rho$, with $J_o \equiv D_v c_v/l_c$. With these choices for the length and velocity scales, the time scale is $t_c = l_c/v_c = R\rho/J_o$. The characteristic stress scale is $\tau_c = \mu J_o/(R\rho)$. The dimensionless groups that show up here are the Capillary number, $Ca = \mu v_c/\sigma = \mu J_o/\rho\sigma$, the Peclet number, $Pe = l_c v_c/D_p = RJ_o/\rho D_p$, and the Damkohler number, $Da = k_d l_c/D_p = k_d R/D_p$. The Capillary number measures the importance of viscous force relative to surface tension force, the Peclet number measures the importance of convective particle transfer relative to diffusive particle transfer, and the Damkohler number measures the importance of the deposition rate relative to the particle diffusion rate.

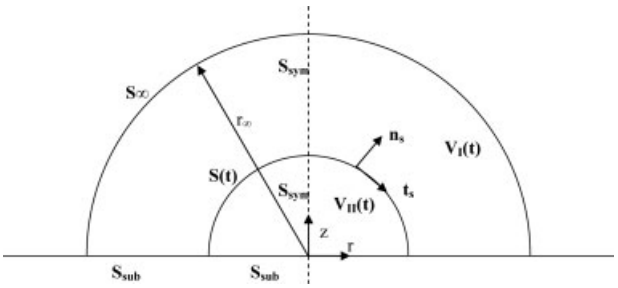

Figure 2. The physical domain of the liquid drop and the vapor above the drop.

The origin of the cylindrical coordinate is fixed and located at the center of the drop on the substrate.

Governing equations, boundary conditions, and initial conditions

The system includes the area above the drop, V_I, and the area inside the drop, V_{II}, as described in Figure 2. The vapor concentration distribution is governed by Laplace equation assuming that the vapor concentration quickly reaches steady state,

$$\nabla^2 c = 0 \text{ in } V_I(t), \tag{1}$$

where c is the dimensionless vapor concentration.

The flow is governed by the continuity equation and Stokes equations. The dimensionless forms of these equations are

$$\nabla \cdot \mathbf{v} = \mathbf{0} \text{ in } V_{II}(t), \tag{2}$$

$$\nabla \cdot \mathbf{T} = 0 \text{ in } V_{II}(t), \tag{3}$$

where $\mathbf{v}$ is the dimensionless velocity, $\mathbf{T} = -p\mathbf{I} + [\nabla\mathbf{v} + (\nabla\mathbf{v})^T]$ is the Newtonian stress tensor, p is the dimensionless pressure, $\mathbf{I}$ is the identity tensor. The particle concentration is governed by the convective diffusive equation,

$$Pe\left(\frac{\partial C_p}{\partial t} + \mathbf{v} \cdot \nabla C_p\right) = \nabla^2 C_p \text{ in } V_{II}(t), \tag{4}$$

where C_p is the dimensionless particle concentration.

Initially, at $t = 0$, the vapor distributes uniformly, the liquid is at rest, and the particle concentration is suspended uniformly in the liquid drop,

$$c = 1 \text{ in } V_I(t), \tag{5}$$

$$\mathbf{v} = 0 \text{ in } V_{II}(t), \tag{6}$$

$$C_p = 1 \text{ in } V_{II}(t). \tag{7}$$

The initial condition for the pressure is the dimensionless pressure inside a hemisphere drop which can be obtained from the dimensionless Young-Laplace equation

$$p = \frac{2}{Ca} \text{ in } V_{II}(t). \tag{8}$$

Equation 1 is solved subject to the boundary conditions that (i) the vapor concentration is the saturated vapor concentration on the interface of the drop, (ii) far away from the drop the vapor concentration is c_∞, (iii) there is no evaporation flux along the solid substrate, and (iv) the evaporation flux is symmetric about the central line,

$$c = 1 \text{ on } S(t) \tag{9}$$

$$c = c_\infty \text{ on } S_\infty \tag{10}$$

$$\mathbf{n} \cdot \nabla c = 0 \text{ on } S_{sub} \tag{11}$$

$$\mathbf{n} \cdot \nabla c = 0 \text{ on } S_{sym} \tag{12}$$

The local flux on the drop interface at radial position r at time t, $J(r, t)$, is calculated by

$$J(r,t) = \mathbf{n_s} \cdot \nabla c \text{ on } S(t) \tag{13}$$

where $\mathbf{n_s}$ is the outward normal unit vector at the liquid–air interface. The evaporation rate at time t, $\dot{m}(t)$, is calculated by integrating the local flux along the interface of the drop.

$$\dot{m}(t) = \int_{S(t)} J(r)\, dS \tag{14}$$

Equations 2 and 3 are solved subject to the boundary conditions that (i) the fluid does not penetrate and slip the solid substrate, (ii) fluid velocity obeys the kinematic boundary condition and (iii) traction boundary condition at the free surface, and (iv), (v) the flow field is symmetric about the central line,

$$\mathbf{v} = 0 \text{ on } S_{SUB}, \tag{15}$$

$$\mathbf{n}_s \cdot (\mathbf{v} - \mathbf{v}_s) = -\mathbf{n}_s \cdot \nabla c \text{ on } S(t), \tag{16}$$

$$\mathbf{n}_s \cdot \mathbf{T} = -\frac{2H}{Ca}\, \mathbf{n}_s \text{ on } S(t), \tag{17}$$

$$\mathbf{n} \cdot \mathbf{T} \cdot \mathbf{t} = 0 \text{ on } S_{sym}, \tag{18}$$

$$\mathbf{n} \cdot \mathbf{v} = 0 \text{ on } S_{sym}, \tag{19}$$

where $\mathbf{v}_s$ is the local velocity of the liquid–air interface, $2H$ is twice local mean curvature of the interface. The evaporation flux is imposed through boundary condition (16). The left hand side of Eq. 16 is evaluated in the liquid system and the right hand side is evaluated in the vapor system.

Equation 4 is solved subject to the boundary conditions that (i) the particle is depositing on the substrate, (ii) there is no particle flux across the drop interface, and (iii) there is also no particle flux across the axis of symmetry,

$$\mathbf{n} \cdot \nabla C_p = -Da\, C_p \text{ on } S_{SUB}, \tag{20}$$

$$\mathbf{n}_s \cdot \nabla C_p - \text{Pe}\, \mathbf{n}_s \cdot C_p \mathbf{v} = 0 \text{ on } S(t), \tag{21}$$

$$\mathbf{n} \cdot \nabla C_p = 0 \text{ on } S_{sym}, \tag{22}$$

The particle flux on the substrate at radial position r and at time t, $J_p(r,t)$, is calculated by

$$J_p(r,t) = -\text{Da}\, C_p \text{ on } S_{SUB} \tag{23}$$

The deposition rate at time t, $\dot{m}_p(t)$, is calculated by integrating the particle flux along the substrate.

$$\dot{m}_{\mathrm{p}}(t) = \int_{S_{\mathrm{sub}}} J_{\mathrm{p}}\, dS \tag{24}$$

The total deposited mass on the substrate at time t, $m_{\mathrm{p}}(t)$, is calculated by multiplying the deposition rate to the time step.

$$m_{\mathrm{p}}(t) = \dot{m}_{\mathrm{p}}(t)\, \Delta t \tag{25}$$

The accumulated deposited mass at the center of the computational element i at position $r = r_{i,\mathrm{node2}}$ and time t, $m_{\mathrm{acc}}(r_{i,\mathrm{node2}},t)$, is calculated by summation of the multiplication of the time step to the integration of the particle flux at that element

$$m_{\mathrm{acc}}(r_{i,\mathrm{node\ 2}}, t) = \sum_{t=0}^{t} \left(\int_{r_{i,\mathrm{node\ 1}}}^{r_{i,\mathrm{node\ 3}}} J_{\mathrm{p}}(r)\, dS \right) \Delta t \tag{26}$$

The particle surface concentration at r_{node2} and time t, $C_{\mathrm{s}}(r_{\mathrm{node2}},t)$, is calculated by

$$C_{\mathrm{s}}(r_{i,\mathrm{node\ 2}}, t) = \frac{m_{\mathrm{acc}}(r_{i+1,\mathrm{node\ 2}}, t) - m_{\mathrm{acc}}(r_{i,\mathrm{node\ 2}}, t)}{\pi(r_{i+1,\mathrm{node\ 2}}{}^2 - r_{i,\mathrm{node\ 2}}{}^2)} \tag{27}$$

Value of parameters

The liquid used here is water. The properties are density, $\rho = 1000$ kg/m^3, surface tension, $\sigma = 72 \times 10^{-3}$ kg/s^2, and viscosity, $\mu = 1 \times 10^{-3}$ kg/m s. The vapor diffusivity, $D_{\mathrm{v}} = 26.1 \times 10^{-6}$ m^2/s, the saturated vapor concentration $c_{\mathrm{v}} = 2.32 \times 10^{-2}$ kg/m^3, $c_{\infty} = 1/r_{\infty}$. The suspended particles are assumed to be spherical with radius of 100 nm, with Stokes Einstein equation, the particle diffusivity is obtained to be $D_{\mathrm{p}} = 4.37 \times 10^{-12}$ m^2/s. For a drop with a radius of $R = 1 \times 10^{-3}$ m, the reference time is $t_{\mathrm{c}} = 1650$ s and reference velocity is $v_{\mathrm{c}} = 4 \times 10^{-6}$ m/s. The capillary number is $Ca = 8.4 \times 10^{-9}$ and the Peclet number is $Pe = 277.28$. The deposition rate constant, k_{d}, is not known, so the Damkohler number is an adjustable parameters.

Numerical Analysis

The governing equations for the vapor concentration distribution above the drop, the fluid dynamics inside the drop, and the particle concentration are solved numerically, using the G/FEM for discretization in the spatial domain and an adaptive finite difference method for discretization in the time domain. For the elliptic mesh generation method, it is convenient to define a cylindrical coordinate system $\{z, r, \theta\}$, whose origin lies at the center of the droplet. For this axisymmetric configuration, the problem is independent of the θ direction. The unknowns need to be solved inside the sessile drop are $p(z, r, t)$, $z(z, r, t)$, $r(z, r, t)$, $v_{\mathrm{z}}(z, r, t)$, $v_{\mathrm{r}}(z, r, t)$, and $C_{\mathrm{p}}(z, r, t)$ and the unknowns need to be solved in the area outside the drop are $z(z, r, t)$, $r(z, r, t)$, $c(z, r, t)$. The unknowns, z, r, v_{z}, v_{r}, c, and C_{p} are expanded using nine-node biquadratic basis functions. The pressure field is expanded using four-node bilinear basis functions. Using the elliptic mesh generation method, the physical domain is discretized into quadrilateral subdomains which are discretized into quadrilateral elements. Each element is mapped onto a unit square in the computational domain. The governing equations are cast as Galerkin Finite Element weighted residuals. The set of nonlinear governing equations are solved via the Newton Raphson's iteration method. The matrix assembled in the G/FEM formulation is solved by using matrix frontal solver.[15] An adaptive implicit time step is used in the time integration scheme. More details about this method will be discussed in the following sections.

Domain discretization and time discretization

The first step is the discretization of the physical domain into quadrilateral subdomains. The procedure used in discretizing the physical domain and the time domain has been discussed in our previous work.[7] The position of the node points was generated by solving a partial differential equation for each computational coordinate. In this work the equations used were developed by Christodoulou and Scriven[16] (Eqs. 28 and 29).

$$\begin{aligned} R^i_{\xi} = & \int_{V(t)} \left[\sqrt{\frac{x_{\xi}^2 + y_{\xi}^2}{x_{\eta}^2 + y_{\eta}^2}} + \varepsilon_{\mathrm{s}} \right] \nabla\xi \cdot \nabla\Phi^i\, J\, d\xi d\eta \\ & - \varepsilon_{\xi} \int_{V(t)} f(\xi)\ \ln(x_{\xi}^2 + y_{\xi}^2)\, \Phi^i_{\xi}\, d\xi d\eta \\ & - M_{\xi} \int_{A(t)} f(\xi)\ \ln(x_{\xi}^2 + y_{\xi}^2)\, \Phi^i_{\xi}\, d\xi = \mathbf{0},\ i = 1, \ldots, N \end{aligned} \tag{28}$$

$$\begin{aligned} R^i_{\eta} = & \int_{V(t)} \left[\sqrt{\frac{x_{\eta}^2 + y_{\eta}^2}{x_{\xi}^2 + y_{\xi}^2}} + \varepsilon_{\mathrm{s}} \right] \nabla\eta \cdot \nabla\Phi^i\, J\, d\xi d\eta \\ & - \varepsilon_{\eta} \int_{V(t)} f(\eta)\ \ln(x_{\eta}^2 + y_{\eta}^2)\, \Phi^i_{\eta}\, d\xi d\eta \\ & - M_{\eta} \int_{A(t)} f(\eta)\ \ln(x_{\eta}^2 + y_{\eta}^2)\, \Phi^i_{\eta}\, d\eta = \mathbf{0},\ i = 1, \ldots, N \end{aligned} \tag{29}$$

N is the number of biquadratic finite element basis functions used in representing the positions,

$$\begin{pmatrix} z \\ r \end{pmatrix} = \sum_{i=1}^{N} \begin{pmatrix} z(t) \\ r(t) \end{pmatrix} \Phi^i(z, r). \tag{30}$$

Finite element analysis

The Galerkin weighted residuals of the Laplace equation, continuity equation, Stokes equations, and particle convective diffusive equation, $R_{i,\mathrm{L}}$, $R_{i,\mathrm{C}}$, $\mathbf{R}_{i,k}$, and $R_{i,p}$ are

$$R_{i,\mathrm{L}} = \int_{V_{\mathrm{I}}(t)} \Phi^i \nabla^2 c\, dV = 0, i = 1, \ldots, N \tag{31}$$

$$R_{i,\mathrm{C}} = \int_{V_{\mathrm{II}}(t)} \Psi^i \nabla \cdot \mathbf{v}\, dV = 0, i = 1, \ldots, M, \text{and} \tag{32}$$

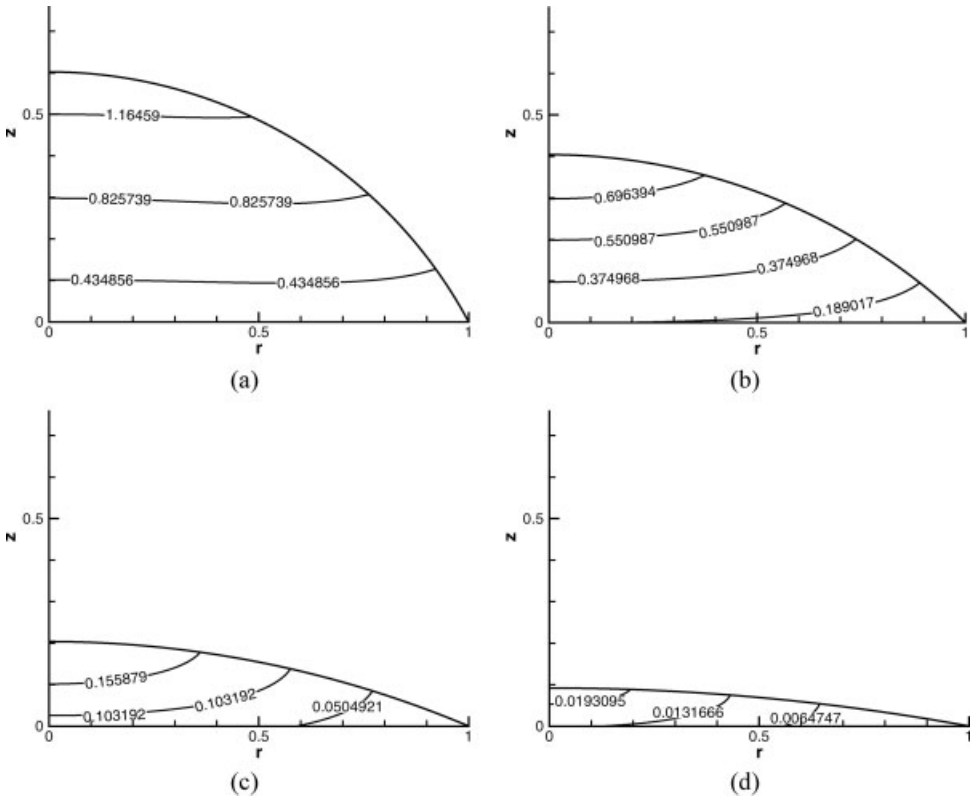

Figure 3. Particle concentration contour and the streamline inside the drop for initial aspect ratio = 0.8, *Pe* = 1, and *Da* = 10.

(a) time = 0.09, (b) time = 0.17, (c) time = 0.24, (d) time = 0.29.

$$\mathbf{R}_{i,k} = \begin{pmatrix} R_{i,z} \\ R_{i,r} \end{pmatrix} = \int_{V_{\Pi}(t)} \Phi^i \mathbf{e}_k \cdot \{\nabla \cdot \mathbf{T}\} dV = \mathbf{0}, i = 1, \ldots N \quad (33)$$

$$R_{i,p} = \int_{V_{\Pi}(t)} \Phi^i \left[Pe \left(\frac{\partial C_p}{\partial t} + \mathbf{v} \cdot \nabla C_p \right) - \nabla^2 C_p \right] dV = 0, \quad i = 1, \ldots, N \quad (34)$$

here $\mathbf{e}_k$ is either $\mathbf{e}_z$ or $\mathbf{e}_r$ and $R_{i,z}$ and $R_{i,r}$ denote the z- and r-Stokes residuals. Here M is the number of bilinear finite-element basis functions used in representing the pressure,

$$p(z, r; t) = \sum_{i=1}^{M} p_i(t)\ \Psi^i(z, r). \quad (35)$$

N is the number of biquadratic finite element basis functions used in representing the vapor concentration and the velocity,

$$c(z, r; t) = \sum_{i=1}^{N} c_i(t)\ \Phi^i(z, r) \quad (36)$$

$$\mathbf{u} = \begin{pmatrix} u_z \\ u_r \end{pmatrix} = \sum_{i=1}^{N} \mathbf{u}_i(t) \Phi^i(z, r) = \sum_{i=1}^{N} \begin{pmatrix} u_{z,i}(t) \\ u_{r,i}(t) \end{pmatrix} \Phi^i(z, r). \quad (37)$$

$$C_p(z, r; t) = \sum_{i=1}^{N} C_{pi}(t)\ \Phi^i(z, r) \quad (38)$$

In the Stokes residuals, the divergence theorem is applied to the stress terms, then the traction boundary is applied to resulting expression. Then the surface divergence theorem is

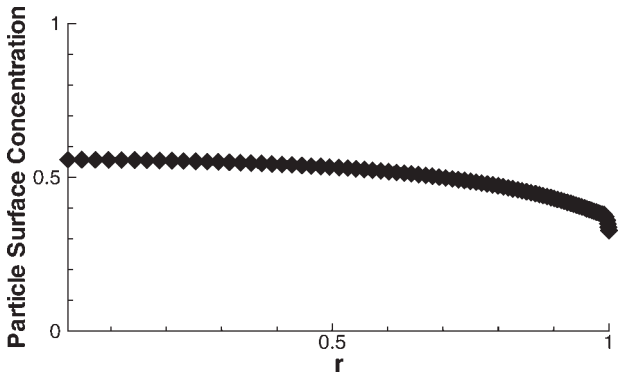

Figure 4. Particle surface concentration on the substrate as a function of the radial position for initial aspect ratio = 0.8, *Pe* = 1, and *Da* = 10.

$r = 0$ is the center of the drop and $r = 1$ is the contact line of the drop.

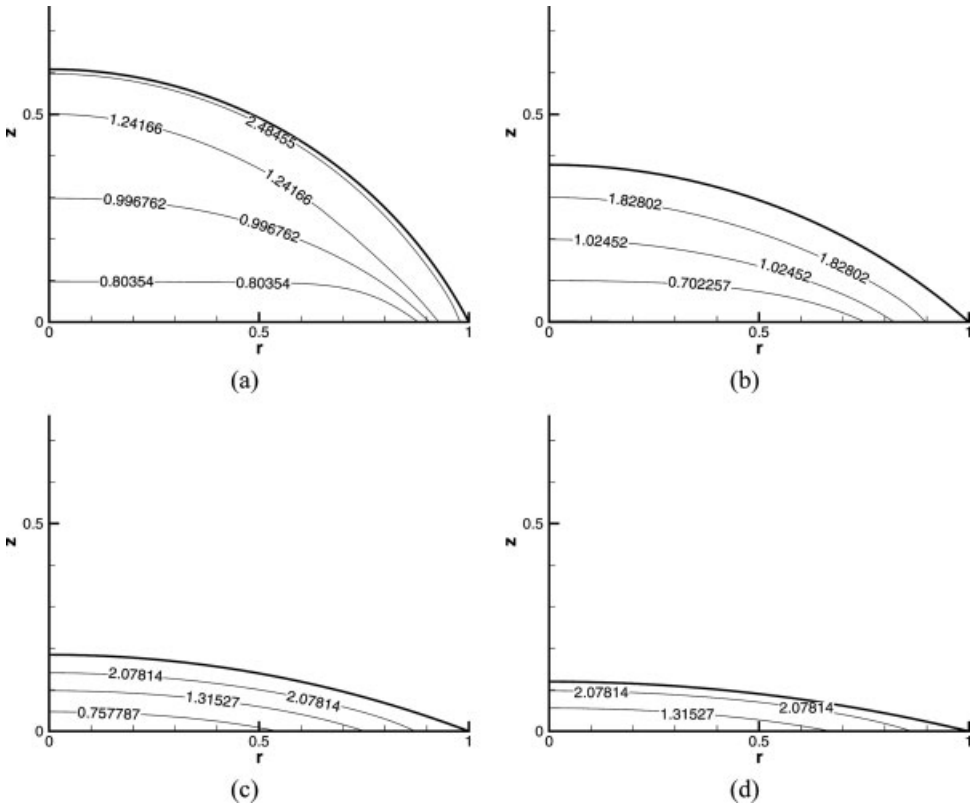

Figure 5. Particle concentration contour and the streamline inside the drop for initial aspect ratio = 0.8, *Pe* = 10, and *Da* = 10.

(a) time = 0.08, (b) time = 0.18, (c) time = 0.25, (d) time = 0.28.

applied to the curvature term in the resulting expression to reduce the order of the equation.

Code validation

The procedure for the code validation is similar to the previous work.[7] Similar mesh configuration is found to be an optimal configuration for the cases that we are solving. Besides monitoring the evaporation time t_{evap}, the final aspect ratio $AR_{final,}$ and the final evaporation rate $\dot{m}_{final}$, we also monitor the particle concentration in the system. The summation of mass in the bulk fluid and the mass on the substrate should be constant. The algorithm is programmed in FORTRAN and is executed in serial on computers with 2.1 GHz AMD Athlon processors.

Results and Discussion

Initially the drop is at its equilibrium shape for a specified initial aspect ratio, and then evaporation flux is imposed along the drop interface. The governing equations are solved numerically using the G/FEM for discretization of the spatial domain and an adaptive finite difference method for discretization in the time domain. The vapor concentration profile surrounding the drop, the drop shape, the fluid velocity, the pressure, and the particle concentration inside the drop are solved simultaneously.

The evaporation flux is increasing closer to the contact line and the fluid is flowing outward to the contact line to compensate the evaporated solvent while fixing the contact line.[7] The influence of the fluid dynamics on the deposition profile is controlled by the importance of convective mass transfer relative to diffusive mass transfer. The surface concentration profile is determined by the competition of the diffusive mass transfer, convective mass transfer, and the particle deposition rate.

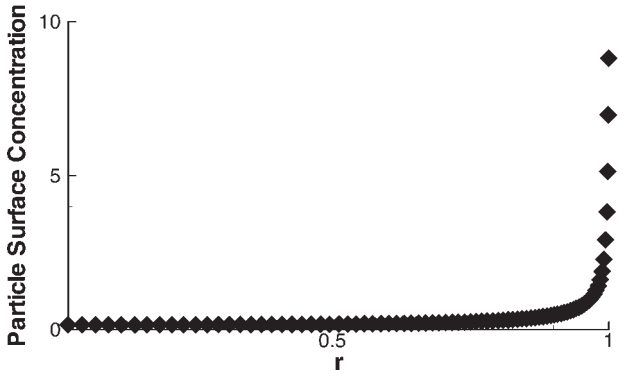

Figure 6. Particle surface concentration on the substrate as a function of the radial position for initial aspect ratio = 0.8, *Pe* = 10, and *Da* = 10.

$r = 0$ is the center of the drop and $r = 1$ is the contact line of the drop.

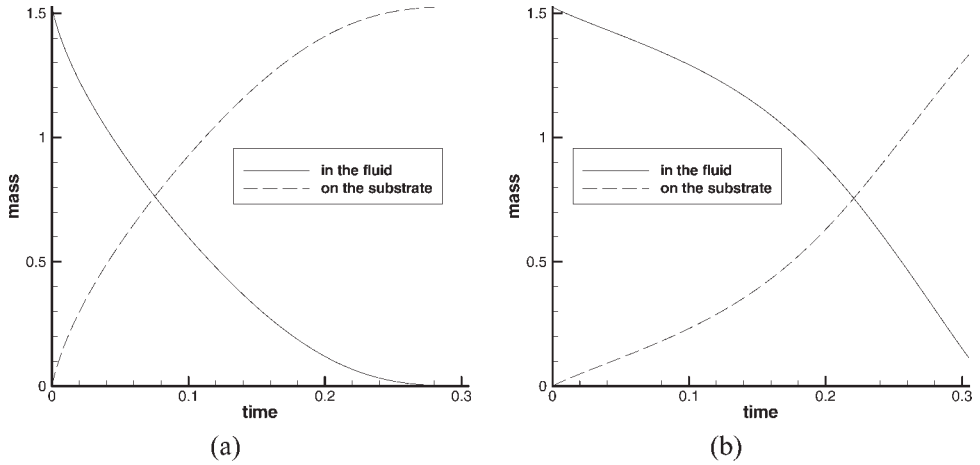

Figure 7. Particle mass as a function of time in the bulk fluid and deposited on the substrate.

(a) $Pe = 1$ and $Da = 10$, (b) $Pe = 10$ and $Da = 10$.

Effect of Peclet number on particle surface concentration profile

At low Peclet number, the diffusive mass transfer dominates over the convective mass transfer. The particle transfer is driven by the particle concentration gradient, the particle motion is not affected much by the fluid flow. The highest particle concentration is on the apex of the drop, then the particle concentration is decreasing toward the substrate of the drop where the particles are deposited to the substrate, and the lowest particle concentration in the liquid is at the

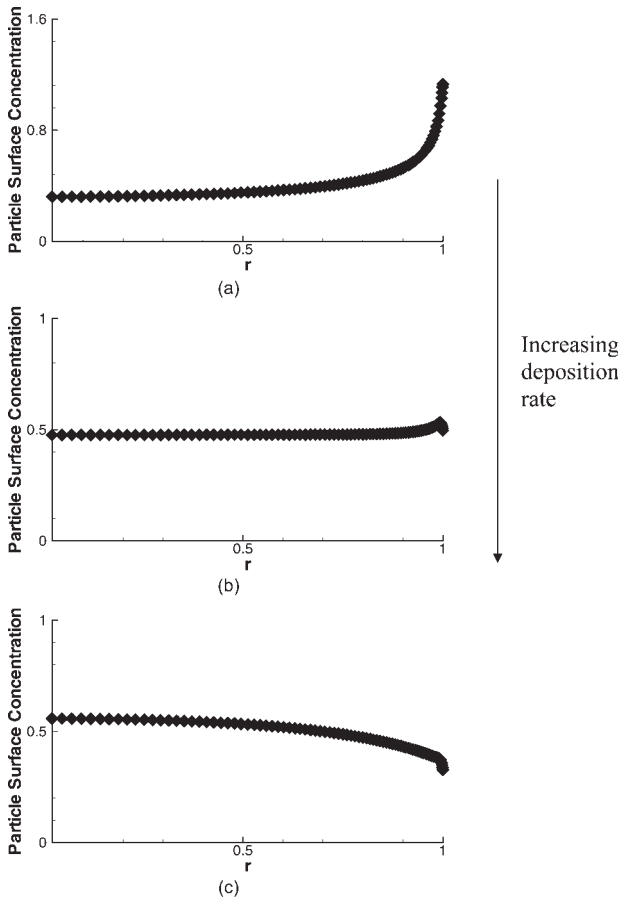

Figure 8. Particle surface concentration profiles for initial drop aspect ratio = 0.8, *Pe* = 1.

(a) $Da = 1$, (b) $Da = 3$, (c) $Da = 10$.

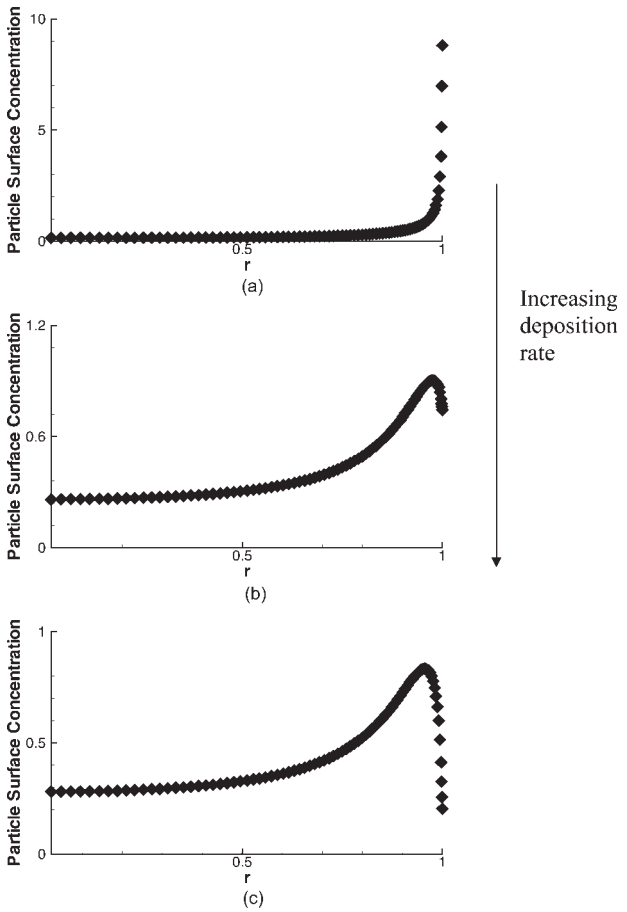

Figure 9. Particle surface concentration profiles for initial drop aspect ratio = 0.8, *Pe* = 10.

(a) $Da = 10$, (b) $Da = 100$, (c) $Da = 1000$.

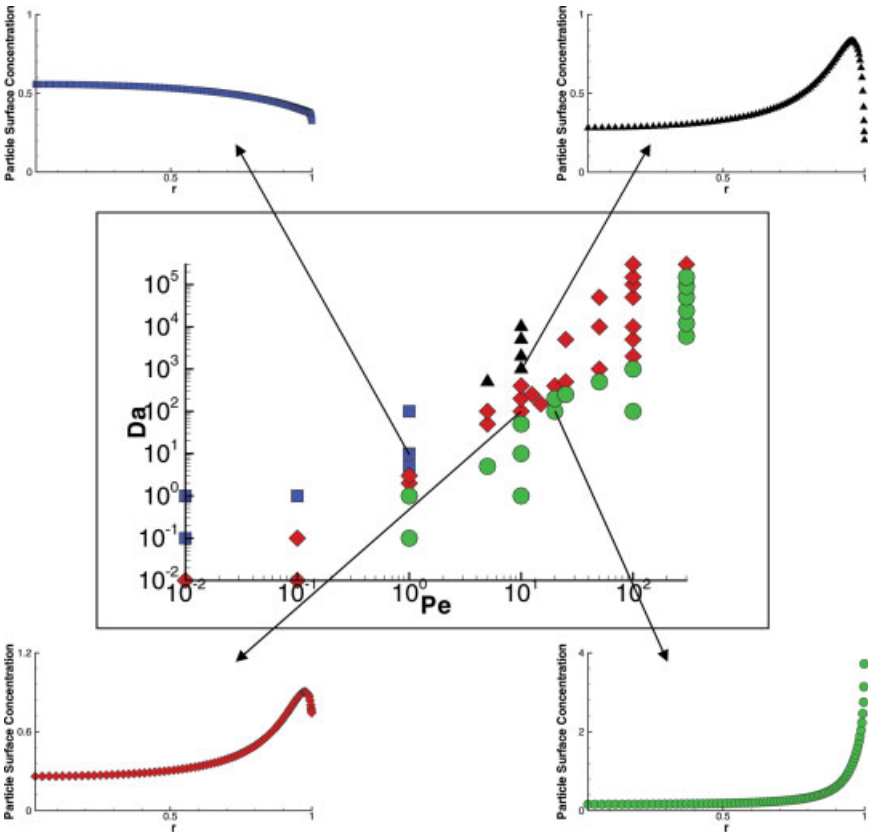

Figure 10. Phase diagram for different particle deposition profile obtained for different *Da* and *Pe*, initial drop aspect ratio = 0.8.

[Color figure can be viewed in the online issue, which is available at www.interscience.wiley.com.]

contact line of the drop (Figure 3). For $Pe = 1$ and $Da = 10$, the surface concentration is almost uniform, the highest surface concentration is at the center of the drop and the lowest is at the contact line (Figure 4).

As the Peclet number is increased, the convective mass transfer is more important relative to the diffusive mass transfer. The particle transfer is influenced more by the fluid flow profile. The particles are carried by the fluid flow toward the drop contact line, which causes accumulation of particles in the area above the contact line. In the bulk fluid, the highest particle concentration is at the contact line and the lowest concentration is along the substrate (Figure 5). On the substrate, the highest surface concentration is at the contact line and the lowest is at the center of the drop (Figure 6).

Figure 7 shows particle mass evolution in the fluid and on the substrate. The particle mass in the fluid is calculated from the integration of the bulk particle concentration throughout the drop volume. The particle mass on the substrate is calculated by the integration of particle flux along the substrate or by the integration of the product of the Damkohler number and the bulk concentration along the substrate. By adding the mass in the bulk and on the substrate, the total mass conservation is monitored. The total mass discrepancy as a function of time is usually less than 1%, unless there is an extremely sharp increase in the deposited particle surface concentration near the contact line of the drop. This problem is resolved by using a finer mesh near the contact line; however, these results in large computational times since the same number of elements are used throughout the computations. Furthermore, the experimental particle deposition profiles tend not to produce the extremely sharp particle surface concentration near the contact line. The total mass discrepancy is therefore acceptable for computations that tend to qualitatively match experimental observations. The integration of the particle flux requires a very refined element close to the substrate. To save computational time, the deposited mass calculation is done by integrating the product of Damkohler number to the particle concentration and the time step size.

At low Peclet numbers, the particles are distributed more uniformly above the substrate, and the particle flux occurs over a large area of the substrate; therefore, takes a shorter time for the particles to be deposited. At higher Peclet numbers, the particles are swept to the area above the contact line, so the deposition is mostly occurring above the contact line. Because the particle deposition occurs over a small area on the substrate, it takes a longer time for the particles to be deposited.

Effect of Damkohler number on particle surface concentration profile

Figure 8 shows the different surface concentration profile for different Damkohler numbers for Peclet = 1. For $Da =$

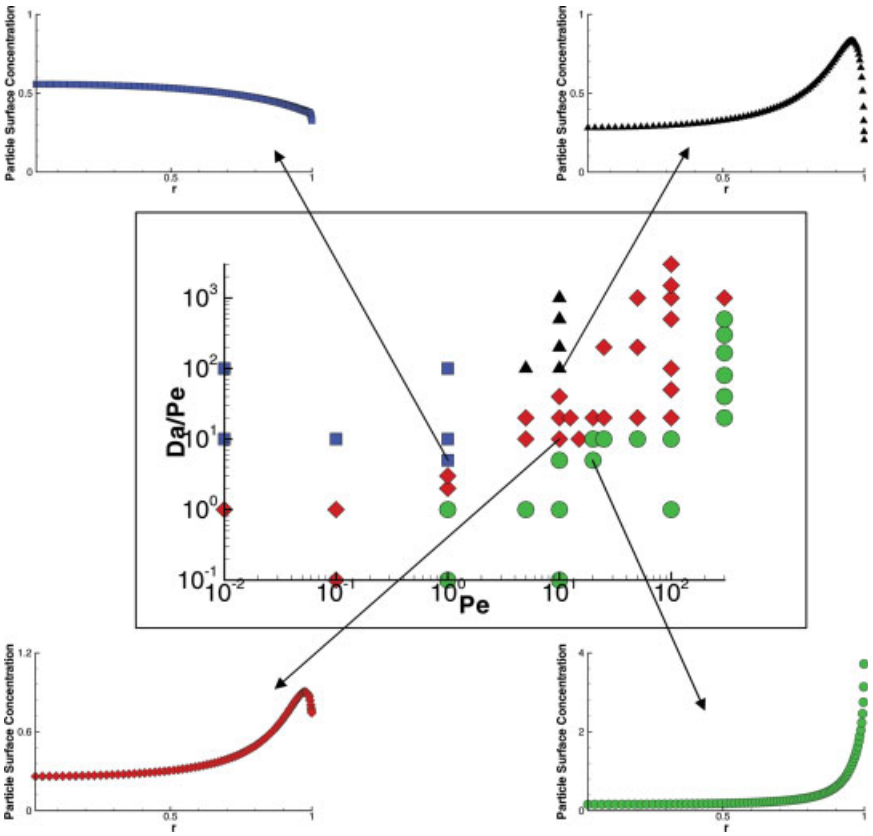

Figure 11. Phase diagram for different particle deposition profile obtained for different *Da*/*Pe* and *Pe*, initial drop aspect ratio = 0.8.

[Color figure can be viewed in the online issue, which is available at www.interscience.wiley.com.]

10, the particles are deposited almost uniformly on the substrate. The highest particle surface concentration is at the center of the drop, and the lowest at the contact line of the drop. For $Da = 3$, which mean at lower deposition rate, some of the particles are swept toward the contact line of the drop forming a shoulder-like profile, the lowest concentration is at the center of the drop, and the highest is at the peak of the shoulder. For $Da = 1$, which mean the deposition rate is lower, the particles are swept by the fluid flow to the contact line before they have time to deposit. In this case, the lowest concentration is at the center of the drop and the highest surface concentration is at the contact line of the drop. So by decreasing the deposition rate, the particles are shifted toward the contact line of the drop.

At a higher Peclet number ($Pe = 10$, Figure 9), the convective mass transfer is more important relative to the diffusive mass transfer. The particles are carried by the fluid flow toward the drop contact line. For $Da = 1000$, the shoulder-like profile is formed, with the highest surface concentration at the peak of the shoulder, and the lowest at the contact line of the drop. Increasing the Peclet number, increases the convective effect. For $Da = 100$, the shoulder is also formed, the highest concentration is still at the peak of the shoulder, but the lowest concentration is at the center of the drop. For $Da = 10$, most of the particles are swept to the contact line. Similar to the low Peclet number case, more particles are deposited near the contact line as the deposition rate decreases.

Parametric study of Peclet and Damkohler numbers

The following particle deposition profiles have been observed which depend on the Peclet and Damkohler numbers: (i) the highest concentration at the center of the drop and the lowest concentration at the contact line of the drop, (ii) the shoulder-like profile with the lowest concentration at the contact line of the drop, (iii) the shoulder-like profile with the lowest concentration at the center of the drop, and (iv) the profile with the highest concentration at the contact line of the drop. Based on these results, more systematic parametric studies of the *Da* vs. *Pe* (Figure 10) and *Da*/*Pe* vs. *Pe* (Figure 11) were done.

In the parametric studies, we can see four regions. The first region is when the deposition rate is high and the diffusive mass transfer dominates over the convective effect. An almost uniform distribution is obtained with the highest particle concentration at the center of the drop and the lowest at the contact line of the drop. The second region is when the deposition rate is high and the convective effect dominates the diffusive effect. A shoulder-like profile is formed with the highest concentration at the peak of the shoulder and the lowest concentration at the contact line of the drop.

The third region is when the deposition rate is low and the diffusive mass transfer dominates the convective effect. A shoulder-like profile is formed with the highest concentration at the peak of the shoulder and the lowest concentration at the center of the drop. The fourth region is when the deposi-

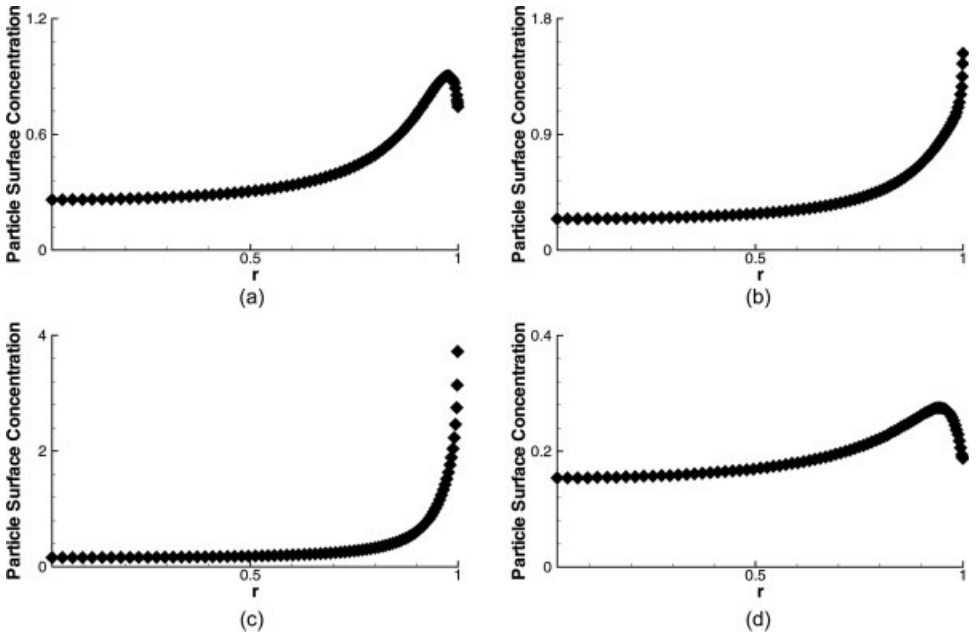

Figure 12. Particle surface concentration profiles.

(a) $Pe = 10$, $Da = 100$, initial aspect ratio = 0.8, (b) $Pe = 10$, $Da = 50$, initial aspect ratio = 0.8, (c) $Pe = 20$, $Da = 100$, initial aspect ratio = 0.8, (d) $Pe = 10$, $Da = 100$, initial aspect ratio = 0.4.

tion rate is low and the convective mass transfer dominates the diffusive mass transfer. Most of the particles are swept to the contact line.

Parameters that control the particle deposition profile

Besides Peclet and Damkohler numbers, there are two other parameters which influence the particle deposition profile, the initial aspect ratio of the drop and the evaporation rate. As we decrease the initial aspect ratio, the evaporation flux closer to the contact line rises, but the evaporation rate drops. As we decrease the evaporation rate, the velocities inside the drop decrease. So, the particles have more time to deposit, before they swept to the contact line of the drop. So, as we decrease the initial aspect ratio of the drop or as we decrease the evaporation rate, the deposition rate increases.

Understanding how the parameters varied with the deposition profile enable us to control the particle deposition profile. For example to shift particles toward center can be done by increasing the deposition rate which is achieved by increasing Damkohler number or decreasing Peclet number or decreasing the initial aspect ratio of the drop or decreasing the evaporation rate. Figures 12 and 13 show different surface concentration profiles that can be obtained by varying those parameters.

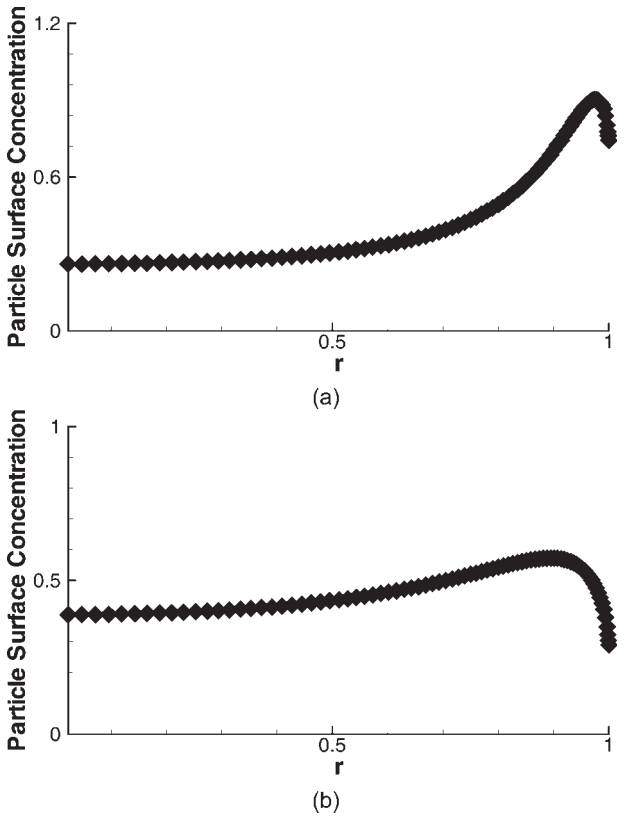

Figure 13. Particle surface concentration profiles for $Pe = 10$, $Da = 100$, initial drop aspect ratio = 0.8, for different evaporation rate.

(a) $c_\infty = 0$, (b) $c_\infty = 0.5$ (lower evaporation rate than case (a)).

Conclusions

We have successfully obtained the particle deposition profile along the substrate during sessile drop evaporation of a particle suspension. The governing equations are solved numerically using the G/FEM for discretization of the spatial domain and an adaptive finite difference method for discreti-

zation in the time domain. The vapor concentration profile around the drop, the drop shape, the fluid velocity and pressure, and the particle concentration profile inside the drop have been solved simultaneously.

Four different particle deposition profiles have been obtained. Several particle deposition profiles which have been obtained experimentally, such as a ring-shaped deposit and uniform particle distribution, are obtained from the numerical simulations. The particle deposition profile is determined by the competition of particle transfer in the bulk (both convective and diffusive mass transfer) and the particle deposition rate along the substrate. The deposition profile can be modified by altering the Peclet number, Damkohler number, the evaporation rate, and the drop initial aspect ratio. Using this numerical model, the deposition profile can be predicted.

Acknowledgments

The authors thank Department of Energy office of basic energy source for supporting this study through grant DE-FG02-02ER45976. The authors acknowledge Dr. Osman A. Basaran and Robert T. Collins for their helpful insight in Finite Element numerical modeling.

Literature Cited

1. Maenosono S, Dushkin CD, Saita S, Yamaguchi Y. Growth of semiconductor nanoparticle ring during the drying of a suspension droplet. *Langmuir*. 1999;15:957–965.
2. Chopra M, Li L, Hu H, Burns MA, Larson RG. DNA molecular configurations in an evaporating droplet near a glass surface. *J Rheol*. 2003;47:1111–1132.
3. Jing J, Reed J, Huang J, Hu X, Clarke V, Edington J, Housman D, Anantharaman TS, Huff EJ, Mishra B, Porter B, Shenker A, Wolfson E, Hiort C, Kantor R, Aston C, Schwartz DC. Automated high resolution optical mapping using arrayed, fluid-fixed DNA molecules. *Proc Natl Acad Sci USA*. 1998;95:8046–8051.
4. Picknett RG, Bexon R. Evaporation of sessile or pendant drops in still air. *J Colloid Interface Sci*. 1977;61:336–350.
5. Hu H, Larson RG. Evaporation of a sessile droplet on a substrate. *J Phys Chem B*. 2002;106:1334–1344.
6. Hu H, Larson RG. Analysis of the microfluid flow in an evaporating sessile droplet. *Langmuir*. 2005;21:3963–3971.
7. Widjaja E, Harris MT. Numerical study of vapor phase-diffusion driven sessile drop evaporation. *Comput Chem Eng*. In press. doi:10.1016/j.compchemeng. 2007.10.014.
8. Deegan RD, Bakajin O, Dupont TF, Huber G, Nagel SR, Witten TA. Capillary flow as the cause of rings stains from dried liquid drops. *Nature*. 1997;389:827–829.
9. Fischer BJ. Particle convection in an evaporating colloidal droplet. *Langmuir*. 2002;18:60–67.
10. Popov YO. Evaporative deposition patterns: spatial dimension of the deposit. *Phys Rev E*. 2005;71:036313-1-0363313-17.
11. Spielman LA, Friedlander SK. Role of the electrical double layer in particle deposition by convective diffusion. *J Colloid Interface Sci*. 1974;46:22–31.
12. Ruckenstein E, Prieve DC. Rate of deposition of brownian particles under the action of london and double-layer forces. *J Chem Soc Faraday Trans 2*. 1973;69:1522–1536.
13. Bowen BD, Levine S, Epstein N. Fine particle deposition in laminar flow through parallel-plate and cylindrical channels. *J Colloid Interface Sci*. 1976;54:375–390.
14. Prieve DC, Ruckenstein E. Rates of deposition of brownian particles calculated by lumping interaction forces into a boundary condition. *J Colloid Interface Sci*. 1976;57:547–550.
15. Hood P. Frontal solution program for unsymmetric matrices. *Int J Numer Methods Eng*. 1976;10:379–399.
16. Christodoulou KN, Scriven LE. Discretization of free surface flows and other moving boundary problems. *J Comput Phys*. 1992;99:39–55.

Manuscript received Jun. 21, 2007, and revision received May 14, 2008.